NOAA Technical Memorandum NWS TDL-55

DISSIPATION, DISPERSION AND DIFFERENCE SCHEMES

Paul E. Long, Jr.

Techniques Development Laboratory
Silver Spring, Md.
May 1975

noaa NATIONAL OCEANIC AND ATMOSPHERIC ADMINISTRATION / National Weather Service

NOAA TECHNICAL MEMORANDA

National Weather Service, Techniques Development Laboratory Series

The primary purpose of the Techniques Development Laboratory of the Office of Systems Development is to translate increases of basic knowledge in meteorology and allied disciplines into improved operating techniques and procedures. To achieve this goal, the laboratory conducts applied research and development aimed at the improvement of diagnostic and prognostic methods for producing weather information. The laboratory performs studies both for the general improvement of prediction methodology used in the National Meteorological Service and for the more effective utilization of weather forecasts by the ultimate user.

NOAA Technical Memoranda in the National Weather Service Techniques Development Laboratory series facilitate rapid distribution of material that may be preliminary in nature and which may be published formally elsewhere at a later date. Publications 1 through 5 are in the former series, Weather Bureau Technical Notes (TN), Techniques Development Laboratory (TDL) Reports; publications 6 through 36 are in the former series, ESSA Technical Memoranda, Weather Bureau Technical Memoranda (WBTM). Beginning with TDL 37, publications are now part of the series NOAA Technical Memoranda, National Weather Service (NWS).

Publications listed below are available from the National Technical Information Service (NTIS), U.S. Department of Commerce, Sills Bldg., 5285 Port Royal Road, Springfield, Va. 22151. Prices vary for paper copy; $1.45 microfiche. Order by accession number, when given, in parentheses at end of each entry.

Weather Bureau Technical Notes

TN 10 TDL 1 Objective Prediction of Daily Surface Temperature. William H. Klein, Curtis W. Crockett, and Carlos R. Dunn, September 1965. (PB-168-590)

TN 11 TDL 2 Hurricane Cindy Galveston Bay Tides. N. A. Pore, A. T. Angelo, and J. G. Taylor, September 1965. (PB-168-608)

TN 29 TDL 3 Atmospheric Effects on Re-Entry Vehicle Dispersions. Karl R. Johannessen, December 1965. (PB-169-381)

TN 45 TDL 4 A Synoptic Climatology of Winter Precipitation From 700-mb. Lows for the Intermountain Areas of the West. Donald L. Jorgensen, William H. Klein, and August F. Korte, May 1966. (PB-170-635)

TN 47 TDL 5 Hemispheric Specification of Sea Level Pressure From Numerical 700-mb. Height Forecasts. William H. Klein and Billy M. Lewis, June 1966. (PB-173-091)

ESSA Technical Memoranda

WBTM TDL 6 A Fortran Program for the Calculation of Hourly Values of Astronomical Tide and Time and Height of High and Low Water. N. A. Pore and R. A. Cummings, January 1967. (PB-174-660)

WBTM TDL 7 Numerical Experiments Leading to the Design of Optimum Global Meteorological Networks. M. A. Alaka and Frank Lewis, February 1967. (PB-174-497)

WBTM TDL 8 An Experiment in the Use of the Balance Equation in the Tropics. M. A. Alaka, D. T. Rubsam, and G. E. Fisher, March 1967. (PB-174-501)

WBTM TDL 9 A Survey of Studies of Aerological Network Requirements. M. A. Alaka, June 1967. (PB-174-984)

WBTM TDL 10 Objective Determination of Sea Level Pressure From Upper Level Heights. William Klein, Frank Lewis, and John Stackpole, May 1967. (PB-179-949)

WBTM TDL 11 Short Range, Subsynoptic Surface Weather Prediction. H. R. Glahn and D. A. Lowry, July 1967. (PB-175-772)

WBTM TDL 12 Charts Giving Station Precipitation in the Plateau States From 700-Mb. Lows During Winter. Donald L. Jorgensen, August F. Korte, and James A. Bunce, Jr., October 1967. (PB-176-742)

WBTM TDL 13 Interim Report on Sea and Swell Forecasting. N. A. Pore and W. S. Richardson, December 1967. (PB-177-038)

WBTM TDL 14 Meteorological Analysis of 1964-65 ICAO Turbulence Data. DeVer Colson, October 1968. (PB-180-268)

WBTM TDL 15 Prediction of Temperature and Dew Point by Three-Dimensional Trajectories. Ronald M. Reap, October 1968. (PB-180-727)

WBTM TDL 16 Objective Visibility Forecasting Techniques Based on Surface and Tower Observations. Donald M. Gales, October 1968. (PB-180-479)

WBTM TDL 17 Second Interim Report on Sea and Swell Forecasting. N. A. Pore and W. S. Richardson, January 1969. (PB-182-273)

WBTM TDL 18 Conditional Probabilities of Precipitation Amounts in the Conterminous United States. Donald L. Jorgensen, William H. Klein, and Charles F. Roberts, March 1969. (PB-183-144)

WBTM TDL 19 An Operationally Oriented Small-Scale 500-Millibar Height Analysis Program. Harry R. Glahn and George W. Hollenbaugh, March 1969. (PB-184-111)

WBTM TDL 20 A Comparison of Two Methods of Reducing Truncation Error. Robert J. Bermowitz, May 1969. (PB-184-741)

WBTM TDL 21 Automatic Decoding of Hourly Weather Reports. George W. Hollenbaugh, Harry R. Glahn, and Dale A. Lowry, July 1969. (PB-185-806)

WBTM TDL 22 An Operationally Oriented Objective Analysis Program. Harry R. Glahn, George W. Hollenbaugh, and Dale A. Lowry, July 1969. (PB-186-129)

WBTM TDL 23 An Operational Subsynoptic Advection Model. Harry R. Glahn, Dale A. Lowry, and George W. Hollenbaugh, July 1969. (PB-186-389)

WBTM TDL 24 A Lake Erie Storm Surge Forecasting Technique. William S. Richardson and N. Arthur Pore, August 1969. (PB-185-778)

(Continued on inside back cover)

NOAA Technical Memorandum NWS TDL-55

DISSIPATION, DISPERSION AND DIFFERENCE SCHEMES

Paul E. Long, Jr.

Techniques Development Laboratory
Silver Spring, Md.
May 1975

UNITED STATES
DEPARTMENT OF COMMERCE
Rogers C. B. Morton, Secretary

NATIONAL OCEANIC AND
ATMOSPHERIC ADMINISTRATION
Robert M. White, Administrator

National Weather
Service
George P. Cressman, Director

Dissipation, Dispersion and Difference Schemes

Paul E. Long, Jr.[1]
Techniques Development Laboratory
National Weather Service, NOAA
Silver Spring, Md. 20910

ABSTRACT. In the first portion of this report we shall study the properties of a number of finite-difference schemes currently used in boundary layer models. We shall do this by introducing a computational diffusion coefficient, K_c, which usually differs markedly from the physical diffusion coefficient, K, for short Fourier component waves. Unless the difference scheme is inconsistent with the differential equation, K_c approaches K for long components. The rate at which K_c/K approaches unity determines the accuracy of the scheme. The behavior of K_c for short and moderate waves is investigated for explicit, pseudo-implicit, and fully implicit difference schemes.

The second portion of this report is concerned with the properties of some implicit advection schemes based upon well-known explicit schemes. The study was motivated by a desire to apply Marchuk's "splitting" technique to two- and three-dimensional systems. The "splitting" technique makes the application of implicit techniques to multi-dimensional systems economically feasible. The dissipative and dispersive properties of the schemes are tabulated.

---

[1] Savannah River Laboratory
E. I. Dupont de Nemours & Co.
Aiken, South Carolina 28901

I. INTRODUCTION

At the Techniques Development Laboratory of the National Weather Service, we are developing a large-scale atmospheric boundary layer model for the prediction of temperature, wind, and humidity from the earth's surface to about 2 km. In figure 1a, the small inner square shows the horizontal extent of our boundary layer system: a grid consisting of 25 x 25 mesh points with a 80-km grid interval which we may eventually telescope to 15 km. The large octagon is the NMC PE (National Meteorological Center Primitive Equation) forecast area. The large and medium squares respectively represent the NMC LFM (limited area fine-mesh) and coarse-mesh boundary layer models.

There are a dozen vertical levels in our model, separated into two portions the contact (or surface) layer and the transition layer (see figure 1b). The contact layer utilizes the constant flux relations of Obukhov which have been determined empirically by Businger [1], Webb [12] and others. These relations are integrated and provide the lower boundary conditions for the transition layer equations.

The transition layer equations are shown below in their real and complex form and include eddy transfer coefficients which allow the diurnal transfer of heat, momentum, and humidity (see table 1 for an explanation of the notation):

$$\frac{\partial \theta}{\partial t} + \vec{V}\cdot\nabla\theta = \frac{\partial}{\partial z}\left(K_T \frac{\partial \theta}{\partial z}\right)$$

$$\frac{\partial q}{\partial t} + \vec{V}\cdot\nabla q = \frac{\partial}{\partial z}\left(K_q \frac{\partial q}{\partial z}\right)$$

$$\frac{\partial u}{\partial t} + \vec{V}\cdot\nabla u = \frac{\partial}{\partial z}\left(K_m \frac{\partial u}{\partial z}\right) + f\,(v - v_g)$$

$$\frac{\partial v}{\partial t} + \vec{V}\cdot\nabla v = \frac{\partial}{\partial z}\left(K_m \frac{\partial v}{\partial z}\right) + f\,(u_g - u)$$

$$\frac{\partial \tilde{T}}{\partial t} + \vec{V}\cdot\nabla\tilde{T} = \frac{\partial}{\partial z}\left(K_T \frac{\partial \tilde{T}}{\partial z}\right)$$

$$\frac{\partial \tilde{W}}{\partial t} + \vec{V}\cdot\nabla\tilde{W} = \frac{\partial}{\partial z}\left(K_m \frac{\partial \tilde{W}}{\partial z}\right) - if\,(\tilde{W} - \tilde{G})$$

$$\tilde{T} = \theta + i\,q \quad ; \quad \tilde{W} = u + i\,v \quad ; \quad \tilde{G} = u_g + i\,v_g$$

$$K_T = K_q \neq K_m$$

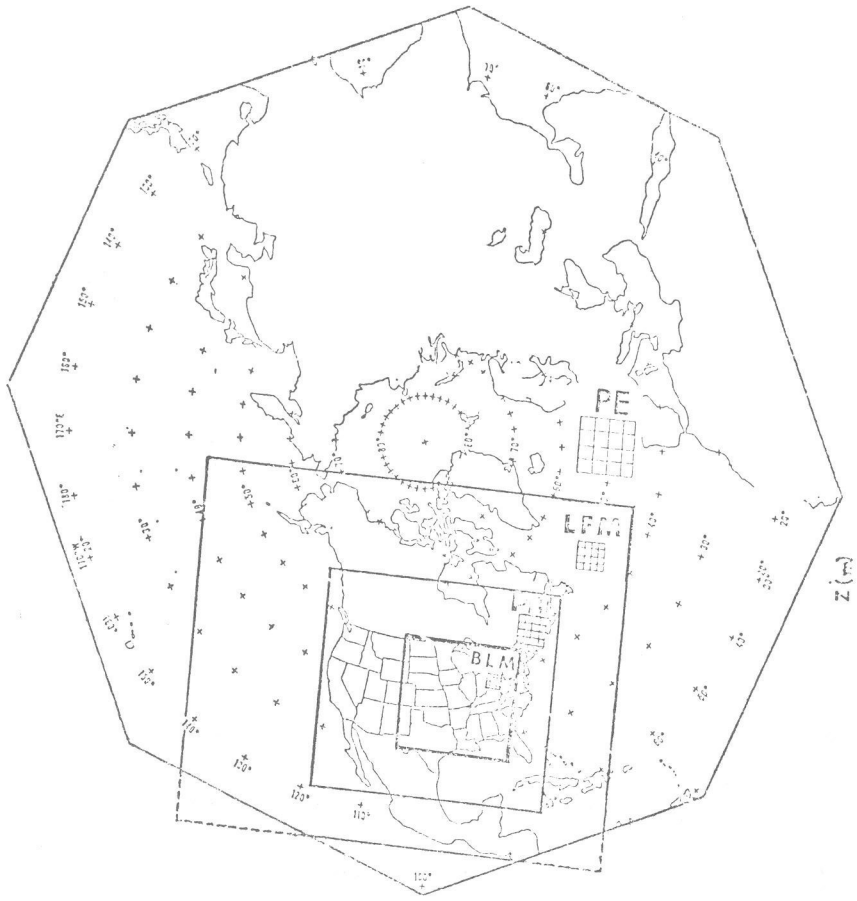

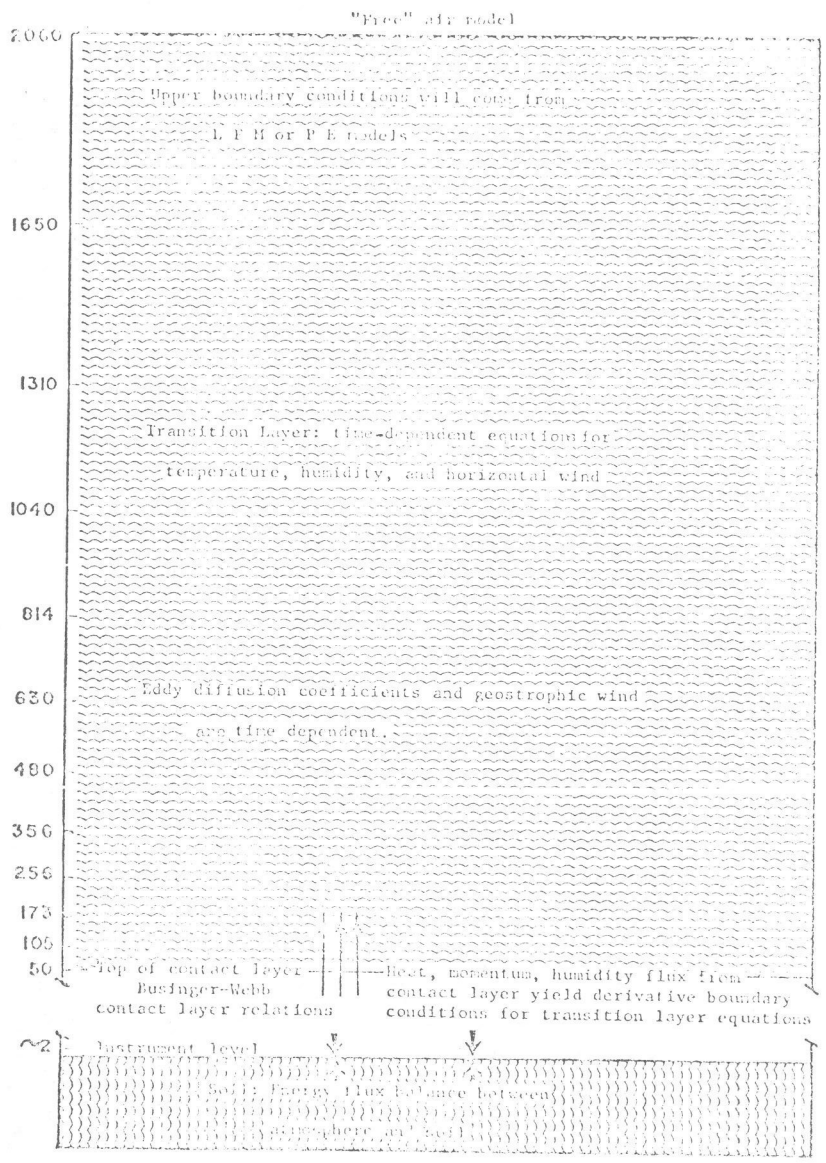

Figure 1.--(a) Coverage of PE, LFM, PBL and BLM models. Grid spacing of models shown by small squares. (b) Vertical schematic of TDL boundary layer model.

Table 1.--Notation

$$Q_j^n = Q(j\Delta z,\ n\Delta t) = Q(z,t)$$

$$\Delta_t Q_j^n = \frac{Q_j^{n+1} - Q_j^n}{\Delta t}$$

$$D_0 Q_j^n = \frac{Q_{j+1}^n - Q_{j-1}^n}{2\Delta Z}$$

$$D_+ Q_j^n = \frac{Q_{j+1}^n - Q_j^n}{\Delta Z}$$

$$D_- Q_j^n = \frac{Q_j^n - Q_{j-1}^n}{\Delta Z}$$

$$D(K_j\ DQ_j^n) = \frac{K_{j-1/2}\ Q_{j-1}^n - (K_{j-1/2} + K_{j+1/2})Q_j^n + K_{j+1/2}\ Q_{j+1}^n}{\Delta Z^2}$$

$$\delta_t\ Q_j^n = \frac{Q_j^{n+1} - Q_j^{n-1}}{2\ \Delta t}$$

$$D\ Q_j^n = \frac{Q_{j+1/2}^n - Q_{j-1/2}^n}{\Delta Z}$$

$$\bar{Q}_j^n = \frac{Q^{n+1} + Q^{n-1}}{2}$$

Table 1.--(Continued)

c: computational phase velocity

f: Coriolis parameter

$\tilde{G}$: complex geostrophic wind

g: amplification factor for a finite difference scheme

g^*: conjugate of g

$g_{\pm}$: amplification factors for "physical" and "computational" modes of a three-level difference scheme

i: $\sqrt{-1}$

j: level index; $Z=j\Delta Z$

K: diffusion coefficient

K_c: computational diffusion coefficient

K_c': effective computational diffusion coefficient shear

K_m, K_q, K_T: diffusion coefficients for momentum, humidity and and heat

L: wavelength of a particular Fourier component

L_o: wavelength for which K_c becomes unbounded

n: time step index; $t=n\Delta t$

Q: general scalar variable

q: specific humidity

R: Courant number; $R= U\Delta t/\Delta x$

$\tilde{T}$: complex temperature-humidity variable; $T=\theta+iq$

t: time

u: east-west wind component

u_g: east-west geostrophic wind component

$\vec{V}$: wind vector

Table 1.--(Continued)

v: north-south wind component

v_g: north-south geostrophic wind component

$\tilde{W}$: complex horizontal wind vector

Δt: time step or increment

ΔZ: level spacing in boundary layer model

λ: wavenumber for Fourier wave used in analyzing finite-difference scheme; $\lambda = 2\pi/L$

μ: weighting factor for Crank-Nicolson diffusion scheme ($0 \leq \mu \leq 1$)

σ: Fourier number, non-dimensional diffusion coefficient; $\sigma = K\Delta t/\Delta Z^2$

σ_o: Fourier number at which pole occurs for $K_c(\lambda, \sigma)$

Θ: potential temperature

The eddy diffusion coefficients in the transition layer are calculated from the O'Brien [8] cubic profile relation which frequently produces daytime maximum values equal to or greater than 100 $m^2 sec^{-1}$. When these large values are used with a large time step and an expanding level system which begins with a level spacing of 50 meters, a considerable strain is placed upon the finite-difference scheme that is used to solve the vertical turbulent transfer equations. Because of the fairly complicated contact layer relations and the energy balance method involving radiation calculations used to compute the surface temperature and local heating, we would like to use a large time step in the numerical integration of the model, as much as one-half hour if possible. We therefore set about studying existing finite-difference schemes to determine their limits of stability and, if absolutely stable, the factors and circumstances attending their eventual degradation.

II. THE NUMERICAL DIFFUSION SCHEMES

We shall study the following finite-difference schemes (see Table 1 for notations):

1. Explicit Schemes

A: $$\Delta_t Q = K D^2 Q_j^n$$

B: $$\Delta_t Q_j^n = K D^2 Q_j^n + \frac{\partial K}{\partial Z} D_o Q_j^n$$

C: $$\Delta_t Q_j^n = K D^2 Q_j^n + \frac{\partial K}{\partial Z} \begin{cases} D_- Q_j^n & ; \quad K' < 0 \\ D_+ Q_j^n & ; \quad K' > 0 \end{cases}$$

D: $$\Delta_t Q_j^n = D (K_j D Q_j^n)$$

Scheme A is a simple two-level explicit scheme for a constant K which may be extended to variable K in several ways as is shown in B, C, and D. Schemes B and D are geometrically different, but for most K profiles give nearly equal solutions. Scheme D is derived by specifying K in between the levels at which Q is computed and by taking the finite-difference analogue of the flux conservation equation. B and C are created by simply taking A and adding shear terms. If K varies linearly with height, B and D give identical results. For arbitrary stratification, B and D differ only by terms of order K" as may be seen by a Taylor series expansion. Scheme C is used in the NMC large-scale atmospheric boundary layer model derived from the Air Force GWC model [4]. It requires a fairly small time step and introduces anomalous computational diffusion through the shear term, as will be described in more detail later.

$$E: \quad \delta_t Q_j^n = KD^2 \, Q_j^n$$

$$F: \quad \delta_t Q_j^n = KD^2 \, Q_j^{n-1} + \frac{\partial K}{\partial Z} D_o \, Q_j^n$$

Scheme E is an attempt to improve upon the one-sided time difference by using a centered difference. Since it uses three time levels, it has a parasitic computational mode which in this case is unstable regardless of how small the time step is taken to be. The scheme was devised by Richardson and is now only of historical and pedagogical interest.

When the K shear vanishes, scheme F formally reduces to A (with $\Delta t \to 2\Delta t$), but has a computational mode. The scheme has been used by Tag [1] in his study of surface temperature in an urban environment and is conditionally stable.

2. Pseudo-implicit Schemes*

$$G: \quad \Delta_t Q_j^n = \frac{K}{\Delta Z^2} \left[Q_{j-1}^n - (Q_j^n + Q_j^{n+1}) + Q_{j+1}^n \right]$$

$$H: \quad \Delta_t Q_j^n = \frac{1}{\Delta Z^2} \left[K_{j-1/2} Q_{j-1}^n - \frac{1}{2} (K_{j+1/2} + K_{j-1/2})(Q_j^{n+1} + Q_j^n) + K_{j+1/2} \, Q_{j+1}^n \right].$$

Scheme G was considered by Mahrt [6] in a numerical study of advective effects on boundary layer flow at low latitudes, and has greater stability than schemes A to F. This scheme may be generalized to variable K by specifying K at half-intervals as in H.

$$I: \quad \Delta_t Q_j^n = \frac{K}{\Delta Z^2} (Q_{j-1}^n - 2 \, Q_j^{n+1} + Q_{j+1}^n)$$

$$J: \quad \Delta_t Q_j^n = \frac{1}{\Delta Z^2} \left[K_{j+1/2} (Q_{j+1}^n - Q_j^{n+1}) - K_{j-1/2} (Q_j^{n+1} - Q_{j-1}^n) \right].$$

Partly because of its absolute stability, scheme I was chosen by Mahrt for his study. Its generalization to variable K, scheme J, was used by Nappo [7] in the numerical boundary layer model devised for use in the Air Resources Atmospheric Turbulence and Diffusion Laboratory.

---

* By pseudo-implicit, we mean a scheme which can be solved explicitly although one or more terms in the spatial derivative is expressed at n + 1.

$$\text{K:}\quad \delta_t Q_j^n = \frac{K}{\Delta Z^2}\left(Q_{j-1}^n - 2\,\bar{Q}_j^n + Q_{j+1}^n\right)$$

$$\text{L:}\quad \delta_t Q_j^n = \frac{K}{\Delta Z^2}\left(Q_{j-1}^n - 2\,\bar{Q}_j^n + Q_{j+1}^n\right) + \frac{\partial K}{\partial Z} D_o\, Q_j^n$$

$$\text{M:}\quad \delta_t Q_j^n = \frac{1}{\Delta Z^2}\left[K_{j+1/2}\, Q_{j+1}^n - \left(K_{j+1/2}+K_{j-1/2}\right)\bar{Q}_j^n + K_{j-1/2} Q_{j-1}^n\right]$$

Scheme K is the widely-used Dufort-Frankel scheme which may be generalized in L or M. L is the scheme used by Estoque [3] in his early boundary layer models and has been widely used by other modelers.

$$\text{N:}\quad \begin{cases} \dfrac{Q_j^{n+1/2} - Q_j^n}{\Delta t} = \dfrac{K}{2\Delta Z}\left(D_+ Q_j^n - D_- Q_j^{n+1/2}\right) & \longrightarrow \\[2ex] \dfrac{Q_j^{n+1} - Q_j^{n+1/2}}{\Delta t} = \dfrac{K}{2\Delta Z}\left(D_+ Q_j^{n+1} - D_- Q_j^{n+1/2}\right) & \longleftarrow \end{cases}$$

$$\text{O:}\quad \begin{cases} \dfrac{Q_j^{n+1/2} - Q_j^n}{\Delta t} = \dfrac{1}{2\Delta Z^2}\left[K_{j+1/2}\left(D_+ Q_j^n\right) - K_{j-1/2}\left(D_- Q_j^{n+1/2}\right)\right] & \longrightarrow \\[2ex] \dfrac{Q_j^{n+1} - Q_j^{n+1/2}}{\Delta t} = \dfrac{1}{2\Delta Z^2}\left[K_{j+1/2}\left(D_+ Q_j^{n+1}\right) - K_{j-1/2}\left(D_- Q_j^{n+1/2}\right)\right] & \longleftarrow \end{cases}$$

Scheme N and its generalization, O, which constitute the Saul'yev [10] alternating method, have only recently been adopted by western modelers. The technique may be applied to alternate time steps, hence its name, or to fractional time steps as shown here. Although formally implicit, the scheme may be solved explicity. The arrows indicate the directions in which the schemes are to be solved. For example, in the first scheme $Q_j^{n+1/2}$ is explicitly computed from $Q_{j-1}^{n+1/2}$, Q_j^n, and Q_{j+1}^n.

3. Implicit Schemes

$$P: \quad \Delta_t Q_j^n = K\left[\mu D^2 Q_j^{n+1} + (1-\mu) D^2 Q_j^n\right]$$

$$Q: \quad \Delta_t Q_j^n = \text{r.h.s. (P)} + \frac{\partial K}{\partial Z} D_o \left[\mu Q_j^{n+1} + (1-\mu) Q_j^n\right]$$

$$R: \quad \Delta_t Q^n = \mu D\left(K_j D Q_j^{n+1}\right) + (1-\mu) D\left(K_j D Q_j^n\right)$$

Schemes P and Q and R are variations of the generalized Crank-Nicolson [2] scheme. Although the schemes are implicit, the systems of unknowns at time step n + 1 form 3-band matrices which allow solutions to be readily calculated [9].

III. ANALYSIS OF THE SCHEMES

The stability and accuracy of computational schemes are usually studied by examining under what conditions their amplification factors remain within or on the unit circle in the complex plane and to which differential equations the difference equations converge for small ΔZ and Δt, with the order of the truncation error determined.

An alternative is to examine the behavior of what we shall call the computational diffusion coefficient, K_c, a function of the grid spacing, time step, wavenumber under consideration, and the particular finite-difference scheme. The computational diffusion coefficient is defined by

$$K_c(\lambda) = -\frac{1}{\lambda^2 \Delta t} \ln|g|$$

and the computational shear of K by

$$\left(\frac{\partial K}{\partial Z}\right)_c = \frac{1}{\lambda \Delta t}\Theta; \quad g = |g| e^{i\Theta}$$

where g is the amplification factor of the scheme, Θ is the argument of g, and λ is the wavenumber. These relations are motivated by assuming the coefficients of the following equation to be quasi-constants and finding the elementary solutions of the differential equation

$$K Q'' + K' Q' = \frac{\partial Q}{\partial t} \; ; \quad \exp\left[-(K\lambda + iK'\lambda)t + i\lambda z\right].$$

The defining relations for $K_c(\lambda)$ and $K'_c(\lambda)$ then follow.

The values for K_c and K'_c may be computed directly or approximated from a power series in λ, for which, apart from the neighborhood of singularities or for large wavenumbers, a few terms are generally sufficient. The amplification factor for diffusion schemes are frequently real, even functions; the shear portions generate odd power series. There are, however, exceptions.

We begin with a simple example: the well-known two-level explicit scheme, A, which becomes unstable when sigma, the Fourier number, defined as $K\Delta t/\Delta Z^2$, exceeds 0.5:

$$\Delta_t Q_j^n = K D^2 Q_j^n$$

$$\sigma = \frac{K\Delta t}{\Delta Z^2} \leq \frac{1}{2} .$$

It follows from

$$g = 1-4\sigma \sin^2 \frac{\lambda \Delta Z}{2}$$

that

$$K_c(\lambda) = -\frac{1}{\lambda^2 \Delta t} \ln \left(1-4\sigma \sin^2 \frac{\lambda \Delta Z}{2}\right)$$

$$= K \left[1-\frac{1}{2} \lambda^2 \Delta Z^2 \left(\frac{1}{6} - \sigma\right)\right] + O(\lambda^4). \qquad (A.1)$$

Instability creates a negative K_c. The deviation of K_c from K is approximately quadratically dependent upon the wave number but for long wavelengths (small wavenumbers) K_c and K become virtually identical.

The λ^2 term in (A.1) may be made to vanish by choosing a time step such that the Fourier number, σ, equals 1/6. The upper curve in figure 2 shows the ratio of K_c to K as a function of wavelength for σ=0.4. When the time step is chosen to make the second term in the power series for λ vanish, the ratio approaches unity much more rapidly than before, as is shown in the lower curve in which σ=1/6. A pole occurring in the upper curve exists whenever $\sigma \geq 1/4$. Within the range of stability of the scheme, a $4\Delta Z$ wave is the longest wave for which the pole can be created.

As noted earlier, schemes B and D, although different geometrically, yield nearly the same results and have a limited stability range. Scheme C uses a one-sided difference for the shear term, introducing anomalous computational K even in the long wavelength limit,

$$K_c \doteq K + \left|\frac{\partial K}{\partial Z}\right| \frac{\Delta Z}{2} \left(1-\left|\frac{\partial K}{\partial Z}\right| \frac{\Delta t}{\Delta Z}\right) .$$

It, too, has a rather restricted stability limitation.

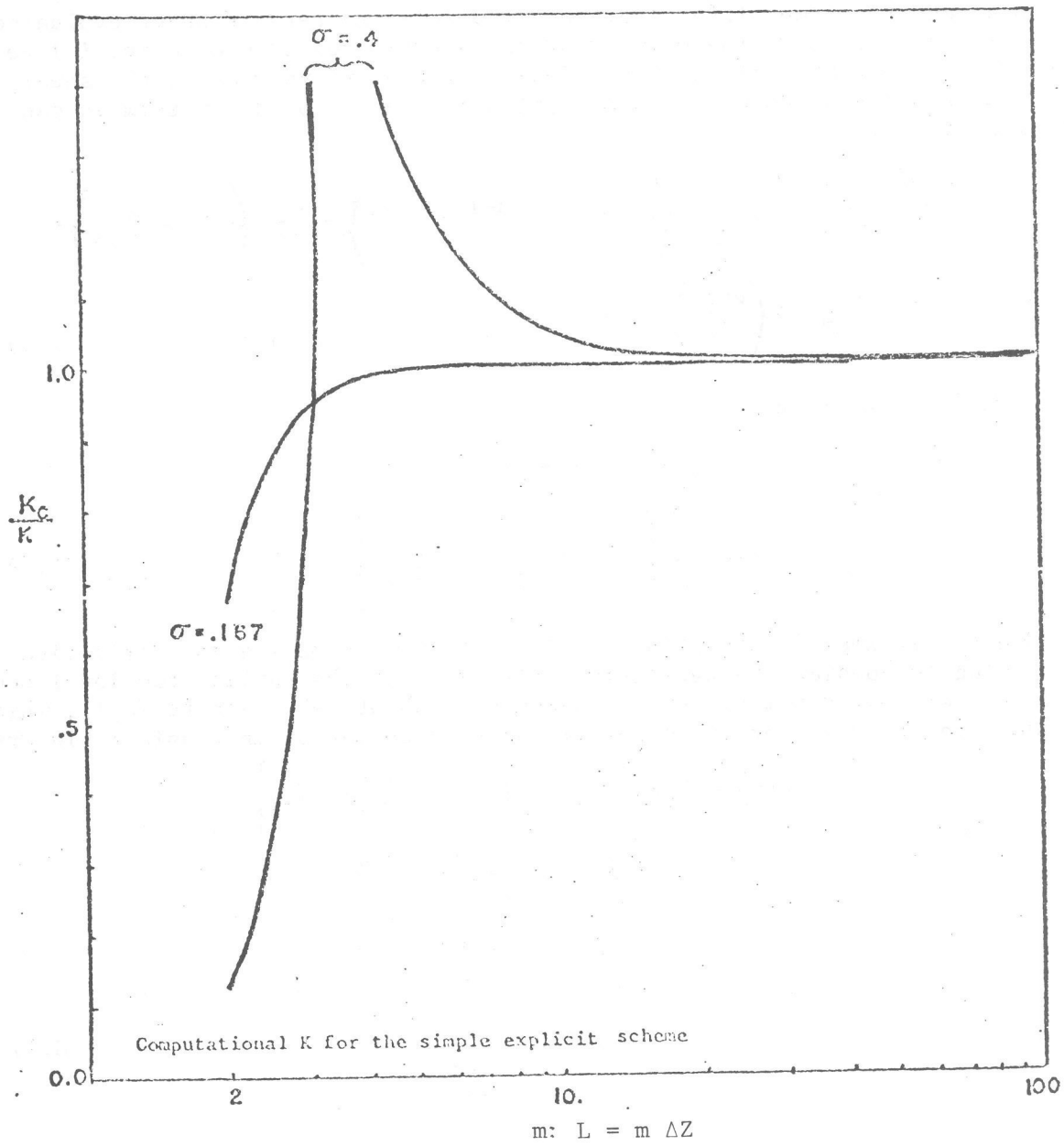

Figure 2.--K_c/K as a function of wavelength for scheme "A".

Tag's scheme F is analogous to the leapfrog advection scheme because it uses a centered time difference, an advection-like term, K shear evaluated at the middle of the time step; requires a two-level scheme to initialize it; and has a computational mode. Unlike the previous scheme, the shear term introduces no anomalous computational K, even to the λ^2 term as can be seen in (F.2):

$$\frac{Q_j^{n+1} - Q_j^{n-1}}{2\Delta t} = \frac{K_j}{\Delta Z^2}\left(Q_{j-1}^{n-1} - 2\,Q_j^{n-1} + Q_{j+1}^{n-1}\right) + \frac{K'}{2\Delta Z}\left(Q_{j+1}^{n} - Q_{j-1}^{n}\right).$$

$$\frac{8K\Delta t}{\Delta Z^2} + \left(\frac{K'\Delta t}{\Delta Z}\right)^2 \leq 1\,, \quad \text{enough for stability} \qquad \text{(F.1)}$$

If (F.1) holds, then

$$|g_{\pm}|^2 = \left|1 - 8\,\sigma \sin^2 \frac{\lambda^2 \Delta Z^2}{2}\right|$$

$$K_c \doteq K\left[1 - \lambda^2 \Delta Z^2\left(\frac{1}{12} - K\frac{\Delta t}{\Delta Z^2}\right)\right] \qquad \text{(F.2)}$$

Mahrt's scheme G averages the middle terms of the spatial derivative, and in doing so doubles the permissible time step of the earlier two level scheme, but not without a price. An expansion of g about $\lambda=0$ leads to (G.1), which then gives a zero-order computational K which may be in considerable error:

$$\Delta t Q_j^n = \frac{K}{\Delta Z^2}\left[Q_{j-1}^n - \left(Q_j^n + Q_j^{n+1}\right) + Q_{j+1}^n\right]$$

$$g = \frac{(1-\sigma) + 2\sigma\cos\lambda\Delta Z}{1+\sigma}$$

$$g \doteq 1 - \frac{\sigma\lambda^2\Delta Z^2}{1+\sigma}$$

$$K_c \doteq \frac{K}{1 + \frac{K\Delta t}{\Delta Z^2}} \qquad \text{(G.1)}$$

For example, when $\sigma=1$ (the stability limit of the scheme) K_c is only 1/2 the desired value. In order to retain the accuracy of the scheme, σ must be kept small, in which case the simpler two-level scheme A would suffice.

Now, it is easy to see that whenever $\sigma \geq 1/3$, singularities occur in K_c for some wavelength beginning with the $2\Delta Z$ waves for $\sigma=1/3$ and extending to the $4\Delta Z$ waves when $\sigma=1$. For a given σ_o, the wavelength L_o which is totally damped is given by

$$L_o = \frac{2\pi\Delta Z}{\cos^{-1}\left(\frac{\sigma_o - 1}{2\sigma_o}\right)}$$

Those waves shorter than L_o undergo a sign reversal at each time step. Variable K can be handled by scheme H ,

$$\Delta_t Q_j^n = \frac{1}{\Delta Z^2}\left[K_{j-1/2}Q_{j-1}^n - \frac{1}{2}\left(K_{j+1/2} + K_{j-1/2}\right)\left(Q_j^{n+1} + Q_j^n\right) + K_{j+1/2}Q_{j+1}^n\right]$$

By evaluating the middle term of the diffusion expression completely at time level n + 1, absolute stability is achieved but at an even greater cost in accuracy than in the preceding scheme. The amplification factor has a magnitude less than unity for all possible K, Δt, ΔZ, and wavenumbers (see I.1), but the expansion about $\lambda=0$ reveals even poorer fidelity than Mahrt's previous scheme. For extremely large values of σ, $K_c=1/2\,\frac{\Delta Z^2}{\Delta t}$; therefore K_c ultimately becomes independent of K altogether:

$$\Delta_t Q_j^n = \frac{K}{\Delta Z^2}\left(Q_{j-1}^n - 2\,Q_j^{n+1} + Q_{j+1}^n\right)$$

$$g = \frac{1+\sigma\,\cos\lambda\Delta Z}{1+2\sigma} \qquad \text{(I.1)}$$

$$K_c \doteq \frac{K}{1+2\,\frac{K\Delta t}{\Delta Z^2}} \qquad \text{(I.2)}$$

Total damping occurs for some wavelength, L_o, whenever $\sigma>1/2$. Regardless of the size of σ, waves longer than $4\Delta Z$ are never completely damped. The connecting relation is (I.3). As before, waves shorter than L_o are very badly handled.

$$L_o = \frac{2\pi\Delta Z}{\pi-\cos^{-1}(1/2\,\sigma_o)} \qquad \text{(I.3)}$$

The restriction of totally damped waves to $4\Delta Z$ or less is, unfortunately, not shared by the Crank-Nicolson scheme, and is one of the reasons for the latter's ultimate degradation as Δt is increased.

The extension of I to variable K is carried out in J. When the diffusion coefficients are expanded about the j^{th} level, the shear makes its presence felt by a destabilizing centered difference term. The scheme need not remain stable, but the shear required for instability is apparently great. The computational K' is modified in a manner analogous to the computational K,

$$K_c' \doteq \frac{K'}{1+2\,\frac{K\Delta t}{\Delta Z^2}}$$

The Dufort-Frankel method (scheme K) is a three-level scheme which averages the middle diffusion term between the past and the future. The scheme is well-known to be absolutely stable with the amplification factors given by (K.1):

$$\delta_t Q_j^n = \frac{K}{\Delta Z^2}\left(Q_{j-1}^n - 2\bar{Q}_j^n + Q_{j+1}^n\right)$$

$$g_{\pm} = \frac{2\sigma\cos\lambda\Delta \pm \sqrt{1-4\sigma^2\sin^2\lambda^2\frac{\Delta Z^2}{2}}}{1+2\sigma} \qquad \text{(K.1)}$$

Whenever $\sigma \leq 1/2$, both the g's are real. A calculation of the computational K to zero order yields the correct damping for the physical mode and total damping for the computational mode,

$$\left.\begin{aligned} K_{c+} &\doteq K \\ K_{c-} &\to \infty \end{aligned}\right\} \quad \sigma < \frac{1}{2}\ ,\ \lambda\Delta Z \equiv \beta << 1$$

For higher-order terms (shorter waves), both K_c's depart from their ideal values. The shortest wave of the computational model is completely undamped.

Increasing σ above 1/2 induces an imaginary part to g for certain short waves and creates a false computational shear given by

$$\left(\frac{\partial K}{\partial Z}\right)_c = \pm\frac{1}{\lambda\Delta t}\tan^{-1}\frac{\sqrt{4\sigma^2\sin^2\lambda^2\frac{\Delta Z^2}{2}-1}}{2\sigma\cos\lambda\Delta Z}\ .$$

If one takes the following limit of the shear, $\lambda\to 0$, $\sigma\to\infty$, and $\sigma\beta\to\infty$, then the computational shear becomes simply $\pm\frac{\Delta Z}{\Delta t}$ This is in agreement with the frequently made statement that the Dufort-Frankel scheme becomes consistant with a hyperbolic equation if Δt and ΔZ are reduced in a fixed ratio. One notes that however large σ may be, a wavelength may be found with no false shear associated with it or with longer wavelengths. For intermediate and shorter waves, a calculation for K yields

$$K_c \doteq \frac{1}{2K\lambda^2}\left(\frac{\Delta Z}{\Delta t}\right)^2,$$

that is, the computational K becomes inversely proportional to the physical K.

Accounting for diffusivity variable with height may be accomplished by either adding a shear term directly to the basic equation, as was done by Estoque, or by specifiying K at intermediate levels,

$$\delta_t Q_j^n = \frac{1}{\Delta Z^2}\left[K_{j-1/2}Q_{j-1/2}^n - \left(K_{j+1/2} + K_{j-1/2}\right)\bar{Q}_j^n + K_{j+1/2}\,Q_{j+1}^n\right]$$

Both approaches lead to nearly the same results. Although amplifying solutions are evidently possible, a large local shear is required.

The alternating Saul'yev method (schemes N and O) does not require the retention of past variables or the computation of the first step by a two-level scheme and does not have a computational mode. Written in time-splitting form, the scheme is marched first from the bottom to the top level to get values at $t + 1/2\ \Delta t$, and then downward, using values at $t + 1/2\ \Delta t$ to get values at $t + \Delta t$,

$$\frac{Q_j^{n+1/2} - Q_j^n}{\Delta t} = \frac{K}{2\Delta Z}\left(D_+ Q_j^n - D_- Q^{n+1/2}\right)$$

$$\frac{Q_j^{n+1} - Q_j^{n+1/2}}{\Delta t} = \frac{K}{2\Delta Z}\left(D_+ Q_j^{n+1} - D_- Q_j^{n+1/2}\right)$$

The amplification factors for these steps are given by g_1 and g_2. The over-all amplification factor is the product of the two fractional-step g's and is always real and less than unity. There are no poles in the plot of K_c, save at $L=2\Delta Z$ when $\sigma=1$, and no sign reversals,

$$g_1 = \frac{1+\frac{\sigma}{2}\left(e^{-i\lambda\Delta Z} - 1\right)}{1-\frac{\sigma}{2}\left(e^{i\lambda\Delta Z} - 1\right)} = g_2^*$$

$$g = g_1 g_2 = \frac{\left[1-\frac{\sigma}{2}\left(1-\cos\lambda\Delta Z\right)\right]^2 + \frac{\sigma^2}{4}\sin^2\lambda\Delta Z}{\left[1+\frac{\sigma}{2}\left(1-\cos\lambda\Delta Z\right)\right]^2 + \frac{\sigma^2}{4}\sin^2\lambda\Delta Z}$$

It is intuitively plausible that the exclusive application of either of the asymmetric schemes leads to the eventual accumulation of fairly large errors. The reason is not that the individual schemes produce grossly incorrect computational K; they do not, but rather the individual schemes introduce anomalous K shears. These are caused by the presence of imaginary parts in g_1 and g_2. To the lowest order of calculation, the imaginary parts vanish and appear only for the shorter waves. The false shears are opposed to one another and cancel completely for all wavelengths when the schemes are applied alternately.

The Saul'yev scheme shares with the Dufort-Frankel scheme the problem of inconsistency. Unless $\Delta t/\Delta Z$ vanishes in the limit $\Delta t/\Delta Z^2 \to 0$, the correct computational K will not be recovered. When very large time steps are used, waves of moderate length are badly handled. Using some of the same approximations as in the analysis of the Dufort-Frankel scheme, one can derive the result,

$$K_c \doteq \frac{4}{K\lambda^2}\left(\frac{\Delta Z}{\Delta t}\right)^2$$

which, except for the numerical factor, is identical to the Dufort-Frankel scheme.

When K varies with height, a slight change in the original scheme accomodates the variable K,

$$\frac{Q_j^{n+1/2} - Q_j^n}{\Delta t} = \frac{1}{2\Delta Z}\left(K_{j+1/2}\ D_+\ Q_j^n - K_{j-1/2}\ D_-\ Q_j^{n+1/2}\right)$$

$$\frac{Q_j^{n+1} - Q_j^{n+1/2}}{\Delta t} = \frac{1}{2\Delta Z}\left(K_{j+1/2}\ D_+\ Q_j^{n+1} - K_{j-1/2}\ D_-\ Q^{n+1/2}\right)$$

It can be easily shown that the additional terms taken alone cause g to lie on the unit circle. No anomalous diffusion or amplification is involved.

The stability properties of the generalized Crank-Nicolson scheme [P,Q,and R] are well known. When the factor μ which weights the future and present derivatives is taken greater than 1/2, the scheme is stable for all time steps. For $\mu<1/2$, the scheme is conditionally stable,

$$\Delta_t Q_j^n = K\left[\mu\ D^2\ Q_j^{n+1} + (1-\mu)\ D^2\ Q_j^n\right] \qquad (P.1)$$

$$0 \leq \mu < 1$$

stable for $\mu > \frac{1}{2}$;

stable for $\mu < \frac{1}{2}$ if $\sigma \leq \frac{1}{2(1-2\mu)}$

Although for $\mu>0$ the scheme is implicit and requires the solution of a 3-band system of simultaneous equations, the effort required is well spent, as will be shown in figure 6.

In computing the computational K, an expansion of λ about zero yields a relation whose deviation from K can be reduced to 0 (λ^4) by requiring the expression in the square brackets to vanish,

$$K_c/K = 1 - \frac{\lambda^2\Delta Z^2}{2}\left[\frac{1}{6} - \sigma\ (1-2\mu)\right]$$

The improvement in the computational K is felt even by very small wavelengths as can be seen in figure 3. The lower curve is the scheme with the derivatives computed completely in the future. The ratio $K_c/K=1$ is approached slowly. The upper curve represents the simple explicit scheme which has a pole at the $2\Delta Z$ wave, after which it fairly quickly approaches the correct value. A great improvement is achieved by setting μ equal to the optimum value suggested above (in this case, $\mu=1/6$). As can be seen, even the $3\Delta Z$ wave is well handled. When the value of σ is increased, the optimum value of μ rapidly approaches 1/2.

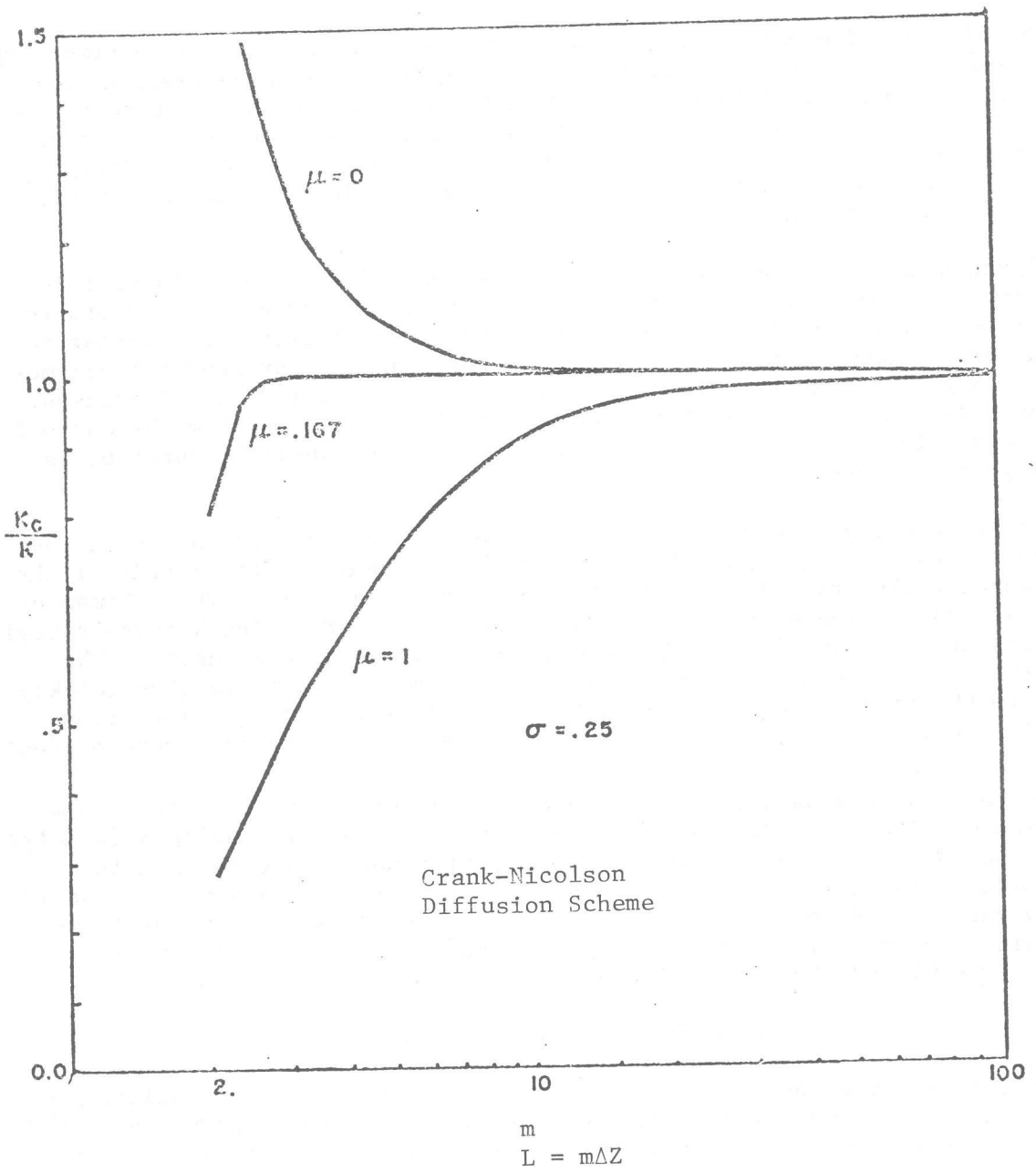

Figure 3.--K_c/K as a function of wavelength for scheme "P".

The ultimate degrading of the Crank-Nicolson scheme for a large time step is caused by the pole which appears at increasingly longer wavelengths and the sign reversal which accompanies it; for wavelengths shorter than the pole-producing wave, the K_c is badly in error and produces solutions of alternating sign. However, the region of poor fidelity of the scheme is considerably narrower for large σ than with the other schemes. The consistency problems which afflict other schemes are absent here.

Figure 4 shows the behavior of several schemes for σ=0.25. Curve 1 is the simple explicit scheme which has good fidelity. Curve 2 represents the Crank-Nicolson and Saul'yev schemes which happened to give very similar results for the small chosen value of σ. Curves 3 and 4 represent the schemes used by Nappo and Mahrt, neither of which approaches unity as L increases. The accurate physical mode of the Dufort-Frankel scheme is shown by curve 5. The computational mode of the Dufort-Frankel scheme, shown by curve 6, is heavily damped even for fairly short waves.

The superiority of the Dufort-Frankel curve is diminished when σ is increased to unity (see figure 5). The Saul'yev scheme creates a pole at the two-grid wave, falls rapidly but then recovers fairly quickly. The schemes of Nappo and Mahrt behave even less accurately than before. The Dufort-Frankel K_c peaks at about wavelength $10\Delta Z$ and then slowly decends to unity. The Crank-Nicolson scheme has complete damping at the $4\Delta Z$ wave and then quickly drops to the correct value. This pattern persists for larger time steps, with the superiority of the Crank-Nicolson scheme becoming even more evident.

The results of a sample calculation of the numerical r.m.s. error as a function of time for a diurnal temperature wave calculation using a 50-meter level spacing are shown in figure 6. The bottom boundary condition is a sinusoidal temperature wave. The supplied diffusion coefficient is a periodically varying O'Brien cubic profile. The Crank-Nicolson scheme performs best with a very small error, followed by the alternating Saul'yev, the Dufort-Frankel, and the Nappo-Mahrt schemes.

IV. THE NUMERICAL ADVECTION SCHEMES

Although a number of accurate explicit advection schemes now exist, the schemes are restrained by stability criteria. On the other hand, the "splitting" method of Marchuk [5] allows stable implicit schemes to be used in place of explicit schemes by reducing a two-or three-dimensional advection equation to a sequence of one-dimensional implicit systems which can be solved relatively easily. We calculated the dissipative and dispersive properties of several conventional difference schemes, making each of them implicit by expressing their spatial derivatives both in the present and the future.

The computational phase errors and diffusion of the explicit schemes were frequently worsened by the conversion to implicit form (see table 2). For example, the largest computational diffusion coefficient for the explicit upstream scheme is less than or equal to the smallest computational diffusion

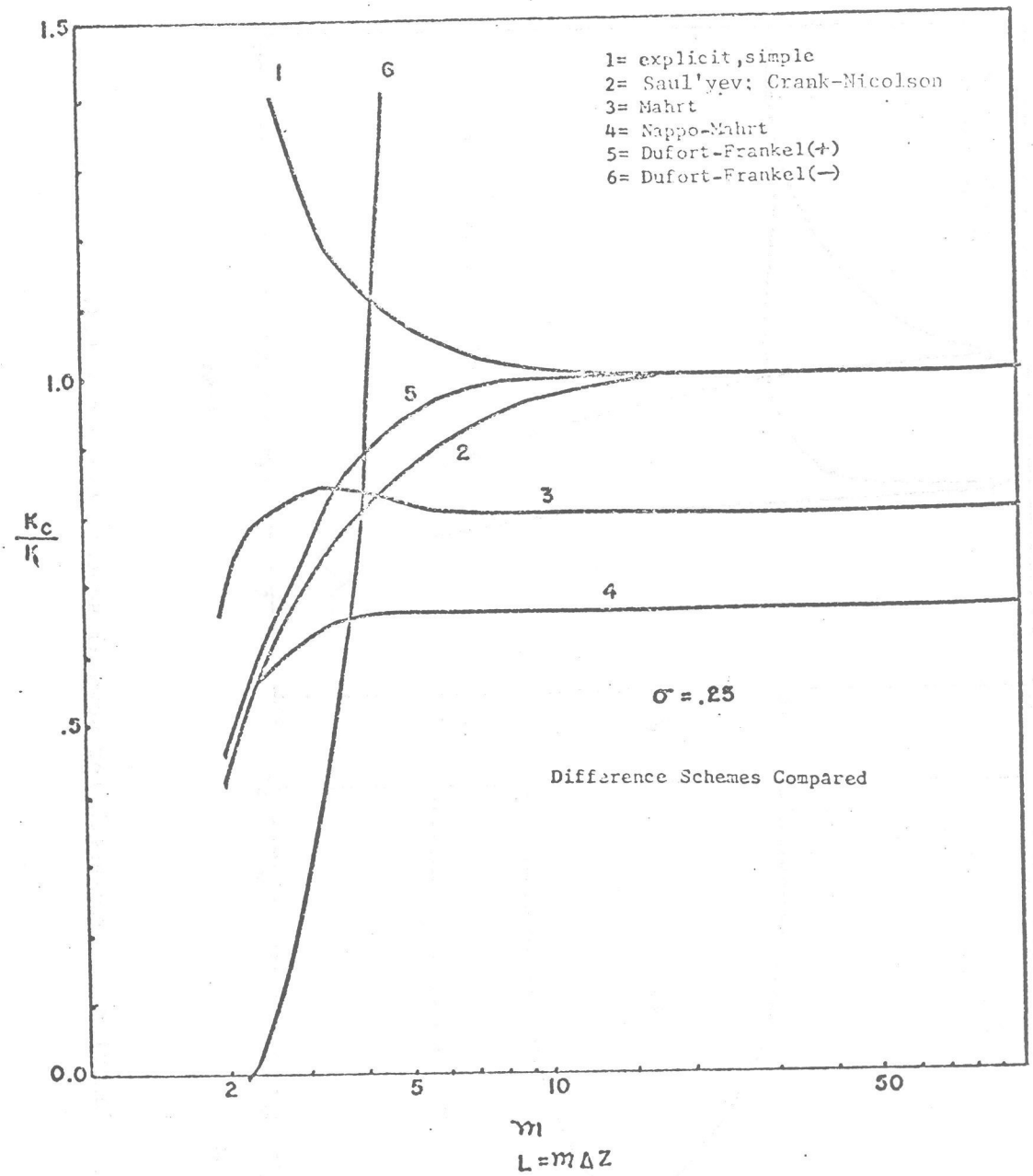

Figure 4.--K_c/K as a function of wavelength for several schemes using $\sigma = 0.25$.

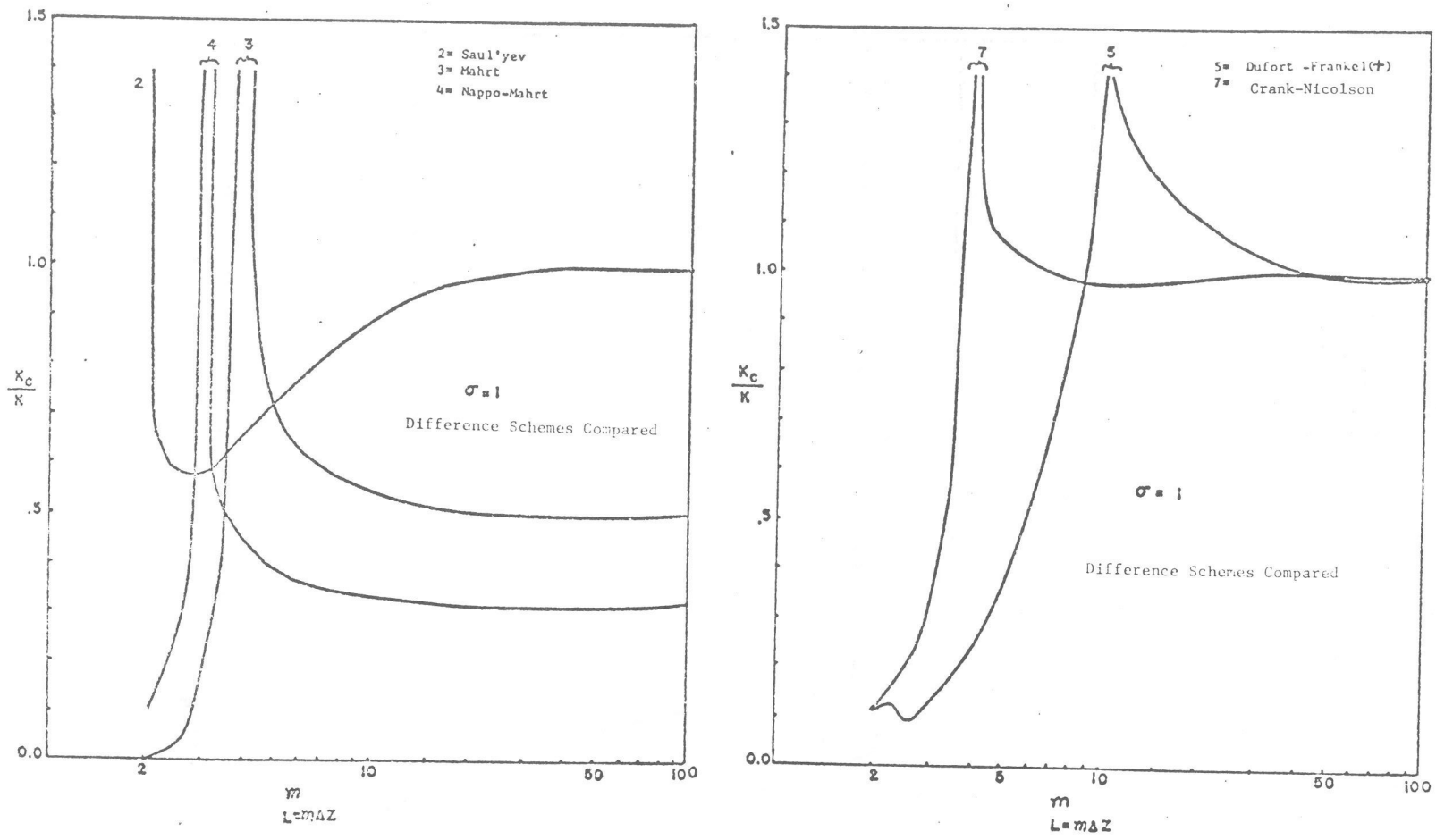

Figure 5.--K_c/K as a function of wavelength for several schemes using σ = 1.0.

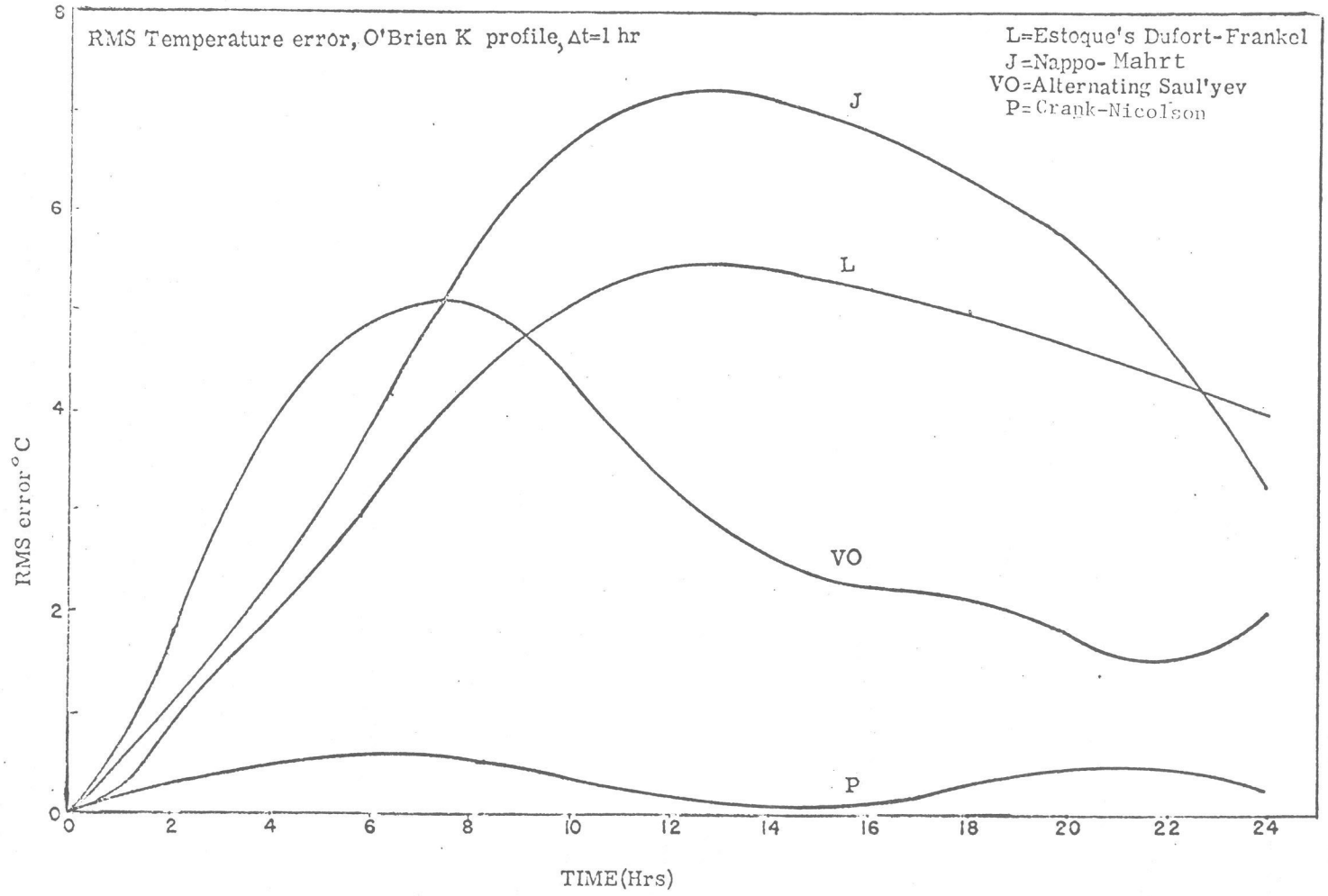

Figure 6.--RMS temperature error as a function of time for several diffusion schemes.

Table 2.--Advection Difference Schemes

Crank-Nicolson:

$$\Delta_t Q_j^n + U \left[\mu D_o Q_j^{n+1} + (1-\mu) D_o Q_j^n \right] = 0$$

Lax-Wendroff:

$$Q_j^{n+1} = Q_j^n - \frac{R}{2} \left[\mu D_o Q_j^{n+1} + (1-\mu) D_o Q_j^n \right] + \frac{R^2}{2} \left[\mu D^2 Q_j^{n+1} + (1-\mu) D^2 Q_j^n \right] = 0$$

Leap-frog:

$$\delta_t Q_j^n + U \left[\mu D_o Q_j^{n+1} + (1-\mu) D_o Q_j^n \right] = 0$$

Saul'yev*:

$$\frac{Q_j^{n+1/2} - Q_j^n}{\Delta t} + \frac{U}{4} \left[D_+ Q_j^n + D_- Q_j^{n+1/2} \right] = 0$$

$$\frac{Q_j^{n+1} - Q_j^{n+1/2}}{\Delta t} + \frac{U}{4} \left[D_+ Q_j^{n+1} + D_- Q_j^{n+1/2} \right] = 0$$

Upstream**:

$$\Delta_t Q_j^n + U D_- \left[\mu Q_j^{n+1} + (1-\mu) Q_j^n \right] = 0$$

Δ^2 Upstream**:

$$\Delta t \, Q_j^n + \frac{U}{\Delta x} \left[\mu \left(3/2 \, Q_j^{n+1} - 2 \, Q_{j-1}^{n+1} + \frac{1}{2} Q_{j-2}^{n+1} \right) + (1-\mu) \left(\frac{3}{2} Q_j^n - 2 \, Q_{j-1}^n + \frac{1}{2} Q_{j-2}^n \right) \right] = 0$$

*Although $|g| < 1$ for all Δt, the sweep becomes unstable when $R > 2$.
**For $U > 0$; obvious change when $U < 0$.

coefficient for the fully implicit version. Weighting the present and future derivatives equally reduces the diffusive effect of the fully implicit equation somewhat.*

Table 3 shows the relative phase velocities of the schemes for $5\Delta X$ waves as a function of the Courant number, that is, the ratio $U\Delta t/\Delta X$. All except the second-order upstream scheme have retarded waves. The retardation becomes acute for large Courant numbers.

Table 4 shows that the non-dimensional computational diffusion coefficient ($K_c\ \Delta t/\Delta X^2$) varies considerably between the schemes and is zero for the Crank-Nicolson and Saul'yev schemes.

Table 5 shows the amplification factors and computational K for a Courant number of 2 as a function of wavelength. Even for long waves, the diffusion is unacceptably high except for the second-order Crank-Nicolson, Saul'yev, and second-order upstream schemes.

Using a higher-order scheme can improve the phase error for small Courant numbers, but the advantage diminishes as the Courant number is increased. In figure 7, contours of relative phase speeds are plotted for second and fourth-order Crank-Nicloson advection schemes. The graph shows that the clear superiority of the fourth-order scheme for small Courant numbers quickly evaporates as the Courant number approaches and passes unity.

Finally, we note that large Courant numbers can create severe problems for the Crank-Nicolson advection scheme at the outflow boundary of a grid. In figure 8, a narrow Gaussian, severely distorted by phase lag, is advected to the outflow boundary of a grid where the outflow conditions are held fixed. A considerable amount of noise is generated locally which eventually propagates back into the forecast area. The use of the upstream advection scheme at the boundary works reasonably well for Courant numbers less than unity but causes a local instability for larger values (figure 9). The fully-implicit upstream advection equation with its heavy damping applied at the boundary greatly improves the outflow properties (figure 10).

V. SUMMARY AND CONCLUSIONS

The concept of a computational diffusion coefficient for a finite-difference equation was introduced as a useful heuristic device. A computational diffusion coefficient represents the amount of diffusion actually introduced by the finite-difference analogue of a partial differential diffusion equation. The coefficient's size depends upon the mesh spacing, time step, and wavelength of Fourier component considered. Unless the difference equation is inconsistent with the differential equation (several examples of inconsistent schemes are given), the computational diffusion coefficient K_c should equal the intended diffusion coefficient in the long wavelength limit. For short Fourier components, K_c may be expected to differ considerably from the intended value. Poles (total damping) frequently appear in plots of K_c versus Fourier wave-length for particular values of K, Δt, and ΔZ. For $L < L_o$,

* In table 2, there is the obvious notational change of Z to X.

Table 3.--C/U as a function of R for $5\Delta x$ waves (μ=.5)

Advection Scheme	$R \equiv U\Delta t/\Delta x$									
	.1	.25	.50	.75	1.00	2.00	3.00	4.00	5.00	10.00
Δ^2 Crank-Nicolson	.756	.753	.743	.727	.706	.605	.509	.432	.373	.217
Lax-Wendroff	.756	.754	.748	.750	.770	.928	.764	.602	.490	.249
Leap-frog	.755	.743	.706	.657	.605	.432	.327	.261	.217	.117
Saul'yev	.757	.757	.759	.761	.764	.770	.751	.546	.356	.089
ΔUpstream	.757	.759	.764	.769	.770	.704	.586	.486	.411	.228
Δ^2Upstream	1.278	1.267	1.230	1.174	1.105	.829	.638	.514	.428	.232

Table 4.--$|g|$, K_c as a function of R for $5\Delta x$ waves (μ=.5)

Advection Schemes		R = $U\Delta t/\Delta x$									
		.1	.25	.50	.75	1.00	2.00	3.00	4.00	5.00	10.00
Δ^2 Crank-Nicolson	$\|g\|$	1.000	1.000	1.000	1.000	1.000	1.000	1.000	1.000	1.000	1.000
	K_c	.000	.000	.000	.000	.000	.000	.000	.000	.000	.000
Lax-Wendroff	$\|g\|$	.993	.958	.849	.707	.567	.400	.585	.722	.806	.945
	K_c	.044	.108	.207	.293	.359	.290	.113	.052	.027	.004
Leap-frog	$\|g\|$	.996	.973	.903	.814	.725	.465	.331	.254	.206	.105
	K_c	.029	.070	.129	.174	.204	.242	.234	.217	.200	.143
Saul'yev	$\|g\|$	1.000	1.000	1.000	1.000	1.000	1.000	1.000	1.000	1.000	1.000
	K_c	.000	.000	.000	.000	.000	.000	.000	.000	.000	.000
ΔUpstream	$\|g\|$	.933	.843	.719	.628	.567	.515	.574	.636	.687	.821
	K_c	.437	.432	.417	.392	.359	.210	.117	.072	.048	.012
Δ^2Upstream	$\|g\|$	.954	.892	.814	.769	.750	.774	.820	.855	.879	.935
	K_c	.300	.291	.261	.222	.182	.081	.042	.025	.016	.004

Table 5.--$|g|$, K_c as functions of $m=L/\Delta x$ for R = 2.

Advection Schemes		m, L = mΔx							
		2	3	4	5	10	20	50	100
Δ^2 Crank-Nicolson	$\|g\|$	1.000	1.000	1.000	1.000	1.000	1.000	1.000	1.000
	K_c	.000	.000	.000	.000	.000	.000	.000	.000
Lax-Wendroff	$\|g\|$	.600	.576	.447	.400	.568	.836	.969	.992
	K_c	.026	.044	.163	.290	.717	.907	.983	.996
Leap-frog	$\|g\|$	1.000	.500	.447	.465	.648	.851	.970	.992
	K_c	0.	.079	.163	.242	.550	.819	.965	.991
Saul'yev	$\|g\|$	1.000	1.000	1.000	1.000	1.000	1.000	1.000	1.000
	K_c	0.	0.	0.	0.	0.	0.	0.	0.
Δ Upstream	$\|g\|$	.333	.378	.447	.515	.753	.914	.985	.996
	K_c	.056	.111	.163	.210	.359	.453	.492	.498
Δ^2Upstream	$\|g\|$	.600	.640	.707	.774	.952	.996	1.000	1.000
	K_c	.026	.051	.070	.081	.062	.022	.004	.001

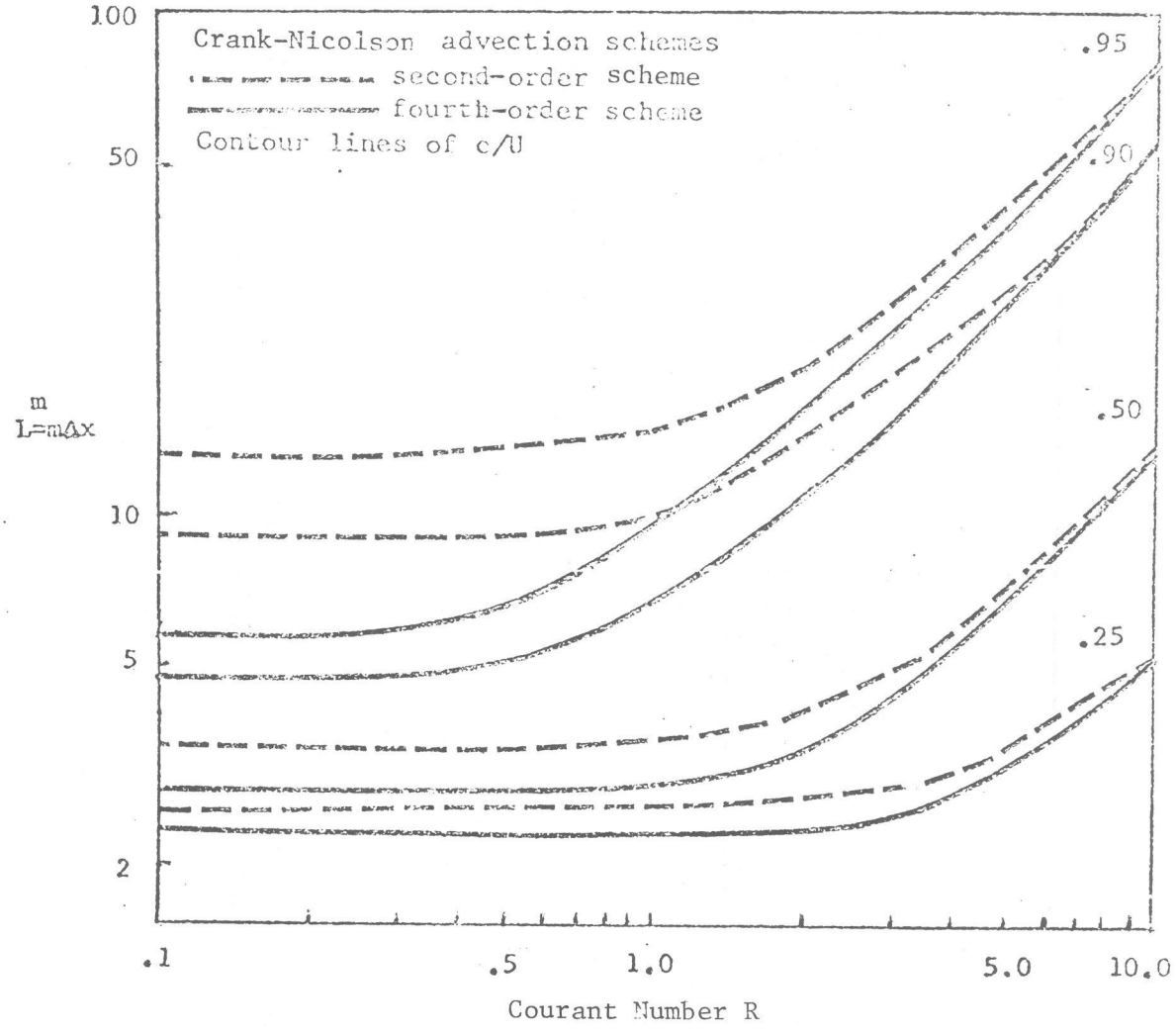

Figure 7.--Contours of phase speeds for Crank-Nicolson second- and fourth-order schemes.

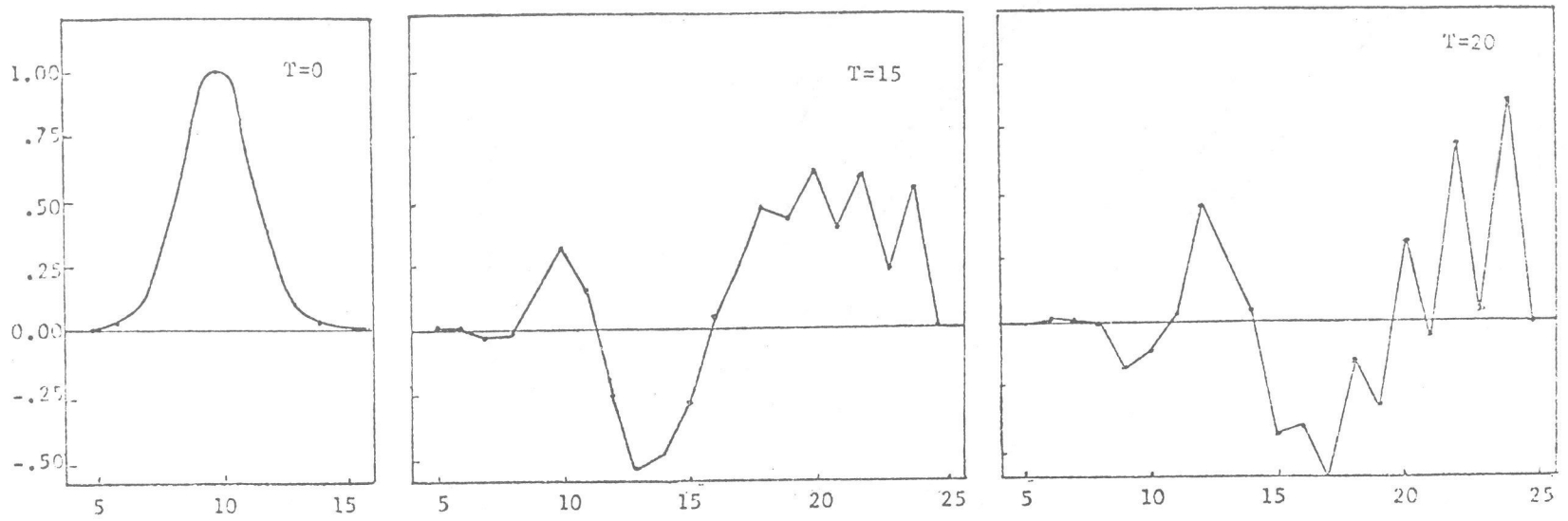

Figure 8.--Evolution of a Gaussian, originally centered at gridpoint number 10 with a half-width of two grid units. Fixed upstream out-flow boundary at gridpoint number 25.

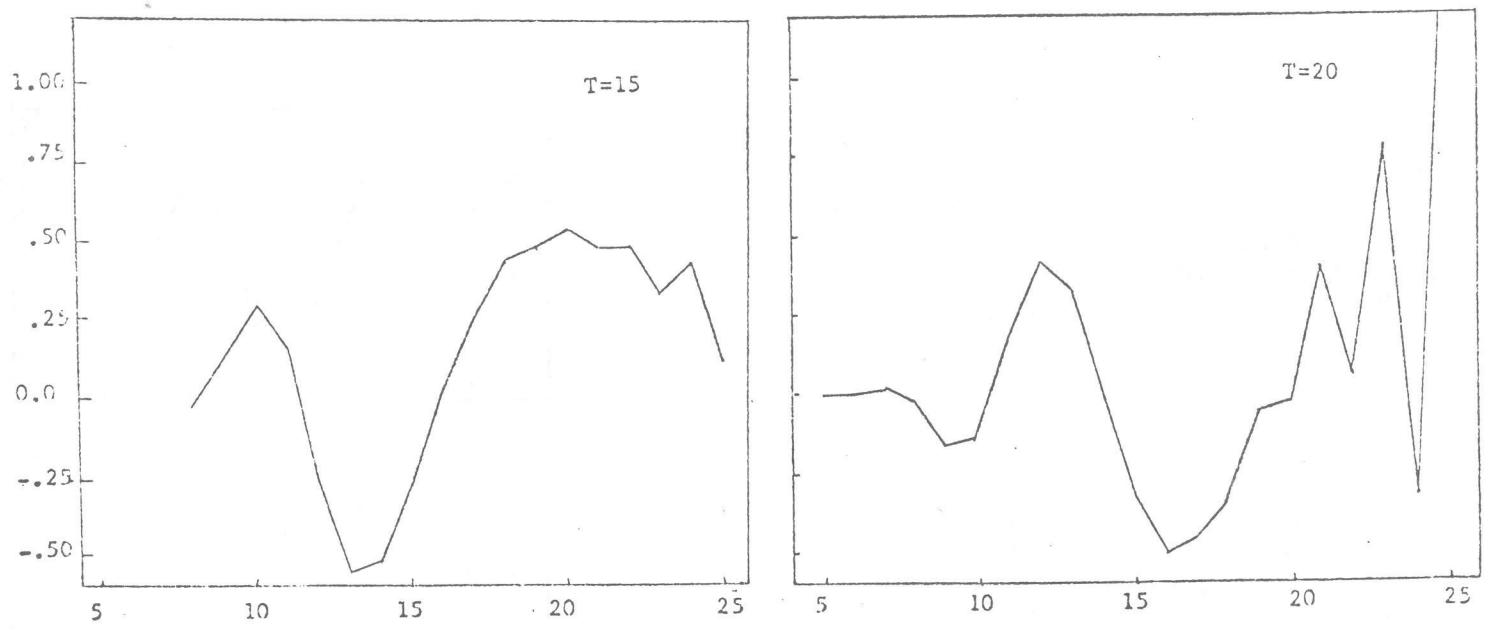

Figure 9.--Similar to figure 8, but explicit upstream boundary condition.

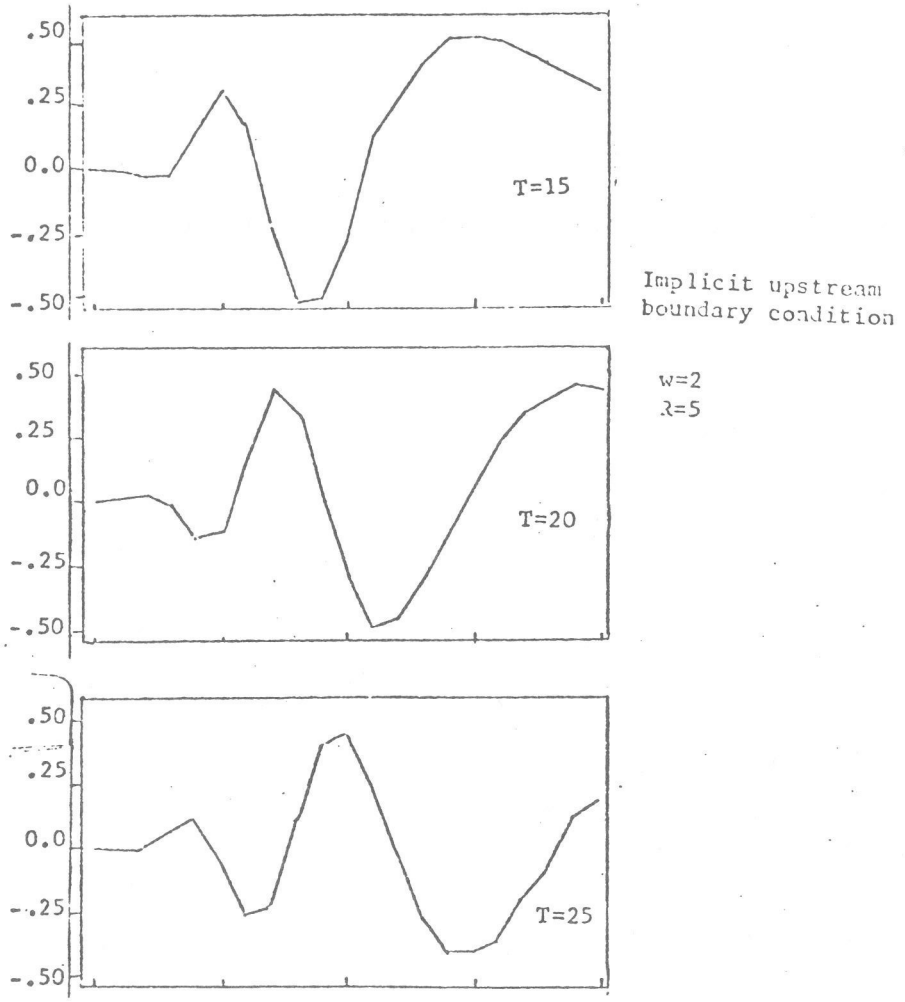

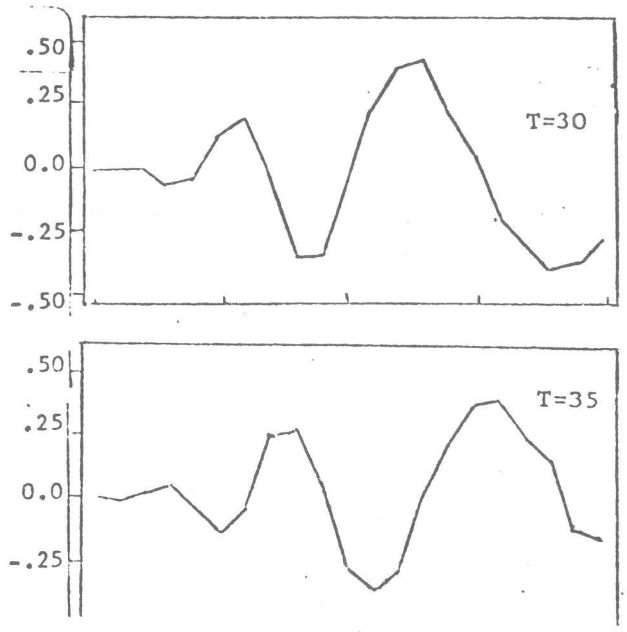

Figure 10.--Similar to figure 9, but implicit upstream boundary condition.

the values at which the poles appear, the schemes commonly cause phase reversal of the waves. If a pole may be manipulated to appear for the two-grid interval waves, the finite-difference scheme will have the useful damping property of removing short waves of questionable accuracy. Unfortunately, this is frequently not possible. However, even with schemes having good stability properties, the poles tend to move to increasingly longer wavelenghts as the time step is increased. Eventually the accuracy of the scheme is destroyed.

The properties of a number of explicit and implicit difference schemes were investigated. Whenever the diffusion coefficients varied with height, heuristic techniques were invoked. Although generally accurate, the explicit schemes normally require small time steps to remain stable. There are several ingenious exceptions in which an explicit scheme is made partially implicit resulting in increased stability. The most successful one investigated is the alternating Saul'yev scheme which, at first glance, appears to be an implicit scheme requiring a system of equations to be solved. In reality, the scheme is solved explicitly by a forward and reverse sweeping process which is stable regardless of the time step. Taken individually, the sweeps introduce an apparent diffusivity shear where none is actually present. Taken together, the false shears cancel exactly.

The Dufort-Frankel scheme is another "pseudo-implicit" scheme which is widely used. This three-level scheme, with its computational mode, has consistency difficulties arising whenever the non-dimensional diffusion coefficient (σ) exceeds 0.5. Apparent diffusivity shears are then created at moderate wavelengths. Larger values of σ produce poles in the "physical" mode's K_c which rapidly shift to longer wavelengths. However, the Dufort-Frankel scheme is accurate and highly efficient if it is pushed only moderately beyond the stability limits of simple explicit schemes.

The generalized Crank-Nicolson scheme is absolutely stable and is the most resistant of all the schemes tested to anomalous computational diffusion. Because the terms in the spatial derivative are evenly balanced in time, the consistency problems which occur with the "pseudo-implicit" schemes are absent. The technique's ultimate degradation is caused by: 1. A pole which progressively infiltrates longer components; 2. The sign flip-flop which occurs behind the pole; 3. The slow recovery of K_c for wavelengths longer than the pole-producing wavelength. Because of the lack of adequate damping for short waves and the onset of sign reversals, the scheme may not work well for "noisy" initial data and rapidly changing boundary conditions. For smooth data and slowly varying boundaries, the Crank-Nicolson scheme may be expected to work quite well even for extremely long time steps.

By use of the "splitting" technique of Marchuk, two-or three-dimensional advection schemes may be easily created and solved. However, except for their stability properties, most of the advection schemes studied here were inferior to their fully-explicit counterparts with respect to both dispersion and dissipation. The fourth-order Crank-Nicolson advection scheme showed considerable improvement over the second-order scheme for small time steps, but the fourth-order scheme's additional accuracy was quickly diminished as the time step was increased.

Acknowledgements

The author wishes to thank Miss Farnese Hicks for her assistance in programming and analysis, Mr. Denis Sakelaris for preparing the figures, and both Mrs. Jocelyn Boss and Mrs. Sandra Swab for typing the text.

REFERENCES

1. Businger, J. A., J. C. Wyngaard, Y. Izumi, and E. F. Bradley, 1971: Flux-profile relationships in the atmospheric surface layer. J. Atmos. Sci., 28, 181-189.

2. Crank, J., and P. Nicolson, 1947: A practical method for numerical solutions of partial differential equations of heat conduction type. Proc. Cambridge Philos. Soc., 43, 50 pp.

3. Estoque, M. A., 1963: A numerical model of the atmospheric boundary layer. J. Geophys. Res., 68, 1103-1113.

4. Hadeen, D. H., and A. L. Friend, 1972: The Air Force Global Weather Central operational boundary-layer model. Boundary-Layer Meteorology, 3, 98-112.

5. Marchuk, G. I., 1964: A new approach to the numerical solution of differential equations of atmospheric processes. WMO-IUGG Symposium on Research and Development Aspects of Long-Range Forecasting, WMO, Tech. Note 16, 212-226.

6. Mahrt, L. J., 1971: A numerical study of advective effects on boundary layer flow at low latitudes. Report, ESSA Grant E-230-68G, Space Science and Engineering Center, The University of Wisconsin, Madison, Wisconsin, 148 pp.

7. Nappo, C. J., 1972: Status report on the ATDL planetary boundary layer numerical modeling program. Air Resources Atmospheric Turbulence and Diffusion Laboratory, NOAA, Oak Ridge, Tennessee, 37 pp. (unpublished manuscript).

8. O'Brien, J. J., 1970: A note on the vertical structure of the eddy exchange coefficient in the planetary boundary layer. J. Atmos. Sci., 27, 1213-1215.

9. Richmyer, R. D., and K. W. Morton, 1967: Difference Methods for Initial-value Problems. Interscience Publishers, New York, 405 pp.

10. Saul'yev, K., 1957: On a method of numerical integration of the equation of diffusion. Doklady Akad., Nauk USSR, 115, 1077 pp.

11. Tag, P. M., 1969: Surface temperatures in an urban environment. Report No. 15, NSF Grant-GA-3956, Dept. of Meteorology, The Pennsylvania State University, University Park, Pa., 22-71.

12. Webb, E. K., 1970: Profile reationships: the long-linear range, and extension to strong stability. Quart. J. R. Met. Soc., 96, 67-90.

(Continued from inside front cover)

WBTM TDL 25 Charts Giving Station Precipitation in the Plateau States From 850- and 500-Millibar Lows During Winter. August F. Korte, Donald L. Jorgensen, and William H. Klein, September 1969. (PB-187-476)

WBTM TDL 26 Computer Forecasts of Maximum and Minimum Surface Temperatures. William H. Klein, Frank Lewis, and George P. Casely, October 1969. (PB-189-105)

WBTM TDL 27 An Operational Method for Objectively Forecasting Probability of Precipitation. Harry R. Glahn and Dale A. Lowry, October 1969. (PB-188-660)

WBTM TDL 28 Techniques for Forecasting Low Water Occurrences at Baltimore and Norfolk. James M. McClelland, March 1970. (PB-191-744)

WBTM TDL 29 A Method for Predicting Surface Winds. Harry R. Glahn, March 1970. (PB-191-745)

WBTM TDL 30 Summary of Selected Reference Material on the Oceanographic Phenomena of Tides, Storm Surges, Waves, and Breakers. N. Arthur Pore, May 1970. (PB-192-449)

WBTM TDL 31 Persistence of Precipitation at 108 Cities in the Conterminous United States. Donald L. Jorgensen and William H. Klein, May 1970. (PB-193-599)

WBTM TDL 32 Computer-Produced Worded Forecasts. Harry R. Glahn, June 1970. (PB-194-262)

WBTM TDL 33 Calculation of Precipitable Water. L. P. Harrison, June 1970. (PB-193-600)

WBTM TDL 34 An Objective Method for Forecasting Winds Over Lake Erie and Lake Ontario. Celso S. Barrientos, August 1970. (PB-194-586)

WBTM TDL 35 Probabilistic Prediction in Meteorology: a Bibliography. Allan H. Murphy and Roger A. Allen, June 1970. (PB-194-415)

WBTM TDL 36 Current High Altitude Observations--Investigation and Possible Improvement. M. A. Alaka and R. C. Elvander, July 1970. (COM-71-00003)

NOAA Technical Memoranda

NWS TDL-37 Prediction of Surface Dew Point Temperatures. R. C. Elvander, February 1971. (COM-71-00253)

NWS TDL-38 Objectively Computed Surface Diagnostic Fields. Robert J. Bermowitz, February 1971. (COM-71-00301)

NWS TDS-39 Computer Prediction of Precipitation Probability for 108 Cities in the United States. William H. Klein, February 1971. (COM-71-00249)

NWS TDL-40 Wave Climatology for the Great Lakes. N. A. Pore, J. M. McClelland, C. S. Barrientos, and W. E. Kennedy, February 1971. (COM-71-00368)

NWS TDL-41 Twice-Daily Mean Monthly Heights in the Troposphere Over North America and Vicinity. August F. Korte, June 1971. (COM-71-00826)

NWS TDL-42 Some Experiments With a Fine-Mesh 500-Millibar Barotropic Model. Robert J. Bermowitz, August 1971. (COM-71-00958)

NWS TDL-43 Air-Sea Energy Exchange in Lagrangian Temperature and Dew Point Forecasts. Ronald M. Reap, October 1971. (COM-71-01112)

NWS TDL-44 Use of Surface Observations in Boundary-Layer Analysis. H. Michael Mogil and William D. Bonner, March 1972. (COM-72-10641)

NWS TDL-45 The Use of Model Output Statistics (MOS) To Estimate Daily Maximum Temperatures. John R. Annett, Harry R. Glahn, and Dale A. Lowry, March 1972. (COM-72-10753)

NWS TDL-46 SPLASH (Special Program To List Amplitudes of Surges From Hurricanes) I. Landfall Storms. Chester P. Jelesnianski, April 1972. (COM-72-10807)

NWS TDL-47 Mean Diurnal and Monthly Height Changes in the Troposphere Over North America and Vicinity. August F. Korte and DeVer Colson, August 1972. (COM-72-11132)

NWS TDL-48 Synoptic Climatological Studies of Precipitation in the Plateau States From 850-, 700-, and 500-Millibar Lows During Spring. August F. Korte, Donald L. Jorgensen, and William H. Klein, August 1972. (COM-73-10069)

NWS TDL-49 Synoptic Climatological Studies of Precipitation in the Plateau States From 850-Millibar Lows During Fall. August F. Korte and DeVer Colson, August 1972. (COM-74-10464)

NWS TDL-50 Forecasting Extratropical Storm Surges For the Northeast Coast of the United States. N. Arthur Pore, William S. Richardson, and Herman P. Perrotti, January 1974. (COM-74-10719)

NWS TDL-51 Predicting the Conditional Probability of Frozen Precipitation. Harry R. Glahn and Joseph R. Bocchieri, March 1974. (COM-74-10909/AS)

NWS TDL-52 SPLASH (Special Program to List Amplitudes of Surges From Hurricanes) II. General Track and Variant Storm Conditions. Chester P. Jelesnianski, March 1974.

NWS TDL-53 A Comparison Between the Single Station and Generalized Operator Techniques for Automated Prediction of Precipitation Probability. Joseph R. Bocchieri, September 1974. (COM-74-11763/AS)

NWS TDL-54 Climatology of Lake Erie Storm Surges at Buffalo and Toledo. N. Arthur Pore, Herman P. Perrotti, and William S. Richardson, December 1974.